# Chirped Coherent Anti-Stokes Raman Scattering for High Spectral Resolution Spectroscopy and Chemically Selective Imaging

**Kelly P. Knutsen, Benjamin M. Messer, Robert M. Onorato, and Richard J. Saykally***

*Department of Chemistry, D31 Hildebrand Hall, University of California, Berkeley, California 94720*

*Received: May 10, 2005; In Final Form: January 26, 2006*

We describe a simple multiplex vibrational spectroscopic imaging technique based on employing chirped femtosecond pulses in a coherent anti-Stokes Raman scattering (CARS) scheme. Overlap of a femtosecond Stokes pulse with chirped pump/probe pulses introduces a temporal gate that defines the spectral resolution of the technique, allowing single-shot acquisition of high spectral resolution CARS spectra over a several hundred wavenumber bandwidth. Simulated chirped (c-) CARS spectra match the experimental results, quantifying the dependence of the high spectral resolution on the properties of the chirped pulse. c-CARS spectromicroscopy offers promise as a simple and generally applicable high spatial resolution, chemically specific imaging technique for studying complex biological and materials samples.

## Introduction

There has been much recent interest in the development of coherent anti-Stokes Raman scattering (CARS) microscopy for chemically selective imaging of complex systems via endogenous chromophores and for quantifying the chemical content of materials in a heterogeneous environment. CARS presents an advantage for imaging those systems wherein fluorescent labeling would cause large perturbations, or perhaps might not even be possible. In this effort, numerous examples of CARS microscopy of complex materials and biological samples have been reported,[1−3] and two thorough reviews of the field were recently published.[4,5] In addition, there have been many proof-of-principle CARS spectroscopy efforts to increase the sensitivity of the technique in order to obtain CARS signals from low abundance samples or from those with cross sections that are small compared to the ubiquitous nonresonant background signal that accompanies nonlinear spectroscopic techniques. Those efforts include employing chirped pulses,[6,7] shaped pulses,[8−10] epi-detection,[11] polarization schemes,[12,13] and heterodyne detection.[14,15]

CARS is a third-order nonlinear process wherein the interaction of three beams, $\omega_p$ and $\omega_{p'}$ (the usually degenerate "pump" and "probe" beams), and $\omega_s$ (the "Stokes" beam) generates the anti-Stokes signal at the frequency $\omega_{as} = 2\omega_p - \omega_s$. By tuning the energy difference $\omega_p - \omega_s$ into coincidence with a vibrational resonance, one can achieve large enhancements in the signal, making it much more sensitive than nonresonant spontaneous Raman spectroscopy. Furthermore, since CARS is a third order nonlinear process, the signal is generated primarily at the tight focus of the overlapped incident laser beams, which allows for depth profiling of the sample. All of these advantages increase the selectivity and sensitivity of CARS microscopy relative to alternative vibrational spectroscopic techniques, and allow for high spatial resolution mapping of complex material and biological samples.

To generate the CARS spectrum, experimental designs often employ relatively narrow bandwidth (picosecond or nanosecond) pulsed lasers to achieve intrinsic sample-limited spectral resolution, with the attendant disadvantages of effecting higher average power (and increased sample heating) and of requiring frequency scanning to generate a spectrum. This increases the acquisition time and makes direct comparisons between peaks in the CARS spectrum more challenging. In contrast, femtosecond pulses have transform-limited bandwidths approaching several hundred wavenumbers, facilitating the simultaneous excitation of multiple vibrational modes. The compromise for this multiplex capability and increased peak power is low spectral resolution relative to typical condensed matter sample line widths (ca. 15 $cm^{-1}$), which reduces the resonant to nonresonant CARS signal, and hence, the chemical selectivity.

An inherent flexibility of CARS spectroscopy is that the three photons used to generate the CARS signal can be a combination of spectrally broad and narrow incident pulses, wherein judicious choice of those pulse widths can generate high spectral resolution multiplex spectra, as shown by the multiplex energy level diagram in Figure 1. Previously described multiplex CARS methods employed broadband (femtosecond) light sources to simultaneously excite several vibrational modes in the sample, followed by a separate narrow bandwidth probe pulse.[3,16] This can be accomplished by using a synchronized femtosecond/picosecond laser combination, wherein the picosecond laser defines the spectral resolution. A disadvantage of this technique is the necessity to synchronize the two separate ultrafast laser systems, which substantially increases the complexity of the experiment. Another approach negates the need for laser synchronization by utilizing the same femtosecond laser as the light source for all three pulses. In that case, the bandwidth of one femtosecond pulse must be reduced. There are two simple methods for accomplishing this. The first is to introduce a filter into the spectrally broad beam to select a small part of the spectrum, effectively converting the femtosecond pulse into a picosecond pulse. This method was previously described by Holtom et al.[17] and recently employed by Kee et al.[18] to achieve high spectral resolution multiplex CARS spectra of materials samples. The other is to disperse the pulse by a pair of prisms or gratings and insert a physical slit into the dispersed beam to remove a small portion of the spectral bandwidth.

* To whom correspondence should be addressed. E-mail: saykally@berkeley.edu. Voice mail: (510) 642-8269. Fax: (510) 642-8566. www.cchem.berkeley.edu/rjsgrp.

10.1021/jp052416a CCC: $33.50 
Published on Web 02/28/2006

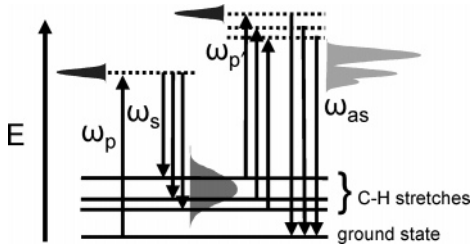


**Figure 1.** Multiplex CARS energy level diagram for the strongest C−H stretches of polystyrene. The pump ($\omega_p$) pulse excites the sample from the ground state into a virtual excited state. The spectrally broad Stokes pulse ($\omega_S$) stimulates the transition from the virtual state, effecting simultaneous excitation of several different vibrational energy levels. Finally, the spectrally narrow probe pulse ($\omega_{p'}$) resolves the manifold of excited transitions by stimulating emission of anti-Stokes photons, which generate the observed CARS spectrum.

In this paper, we expand upon recently described experimental results using a simple variation on the latter design for CARS spectroscopy, wherein the spectral resolution of our instrument is defined by a "temporal gate" rather than by a mechanical slit.[6] By passing a 90 fs pulse between two gratings for four total passes, a linear chirp is induced in the pulse that temporally stretches the pulse to 9.4 ps. The spectral bandwidth of the chirped pulse is the same as the original 90 fs pulse, but it is now dispersed in time, with the blue frequencies leading the red frequencies (a negative chirp). The spectral resolution of the chirped CARS technique arises from the fact that the CARS signal is generated primarily when a chirped pump/probe and transform-limited Stokes pulses overlap in time and space. Therefore, an effective "temporal gate" is introduced into the optical path, since the 90 fs Stokes pulse temporally overlaps with only a small portion (in time) of the much longer 9.4 ps pump/probe pulse. Due to the temporal chirp of the pump/probe pulse, this temporal overlap also corresponds to only a small fraction of the pump/probe (transform limited) frequency bandwidth.

The effective spectral resolution of the CARS output ($\omega_{as}$), in the limiting case that the chirped pump/probe ($\omega_p$) pulse is much longer than the Stokes ($\omega_s$) pulse, is given by

$$\Delta\omega_{spec} = \Delta t_S \frac{\Delta\omega_p}{\Delta t_p} \quad (1)$$

where $\Delta t_S$ is the pulse width of the unchirped $\omega_S$ pulse, $\Delta\omega_p$ is the spectral bandwidth of the chirped $\omega_p$ pulse, and $\Delta t_p$ is the pulse width of the chirped $\omega_p$ pulse. The ratio of $\Delta\omega_p$ to $\Delta t_p$ is the chirp rate of the chirped pulse, the time rate of change of frequency over the extent of the temporally chirped pulse. The resulting effective spectral resolution of the CARS signal, $\Delta\omega_{spec}$, is determined by the frequency bandwidth projected by the temporally short Stokes pulse. This simple relation ignores the dephasing time of the vibrational state, which will limit the achievable spectral resolution for molecular vibrations with long dephasing times, since the chirped pulse continues to interact with the dephasing transition. This challenge to observing high spectral resolution was briefly mentioned by Richter et al. when they employed chirped pulses to achieve high spectral resolution multiplex sum frequency generation, a nonlinear surface specific vibrational spectroscopic technique.[19] This effect will be described in greater detail later.

Chirped pulses have previously been employed in nonlinear optical spectroscopy techniques, often as a means to more readily extract dynamical information from excited electronic states.[20−23] The effect of chirping the femtosecond Stokes pulse on the observed multiplex CARS spectrum when temporally overlapped and synchronized with transform-limited picosecond pump/probe pulses was previously described by Cheng et al.[16] They noted that the overall spectral bandwidth of their CARS signal decreased for decreased chirp rates of the *Stokes* pulse, due to the decreased overlap of the spectral components of the chirped pulse. However, as described below, more interesting effects occur when the *probe* pulse is chirped when employing originally femtosecond pulses for generating CARS signals, namely, the decreased overlap of the spectral components between the chirped probe pulse and the unchirped Stokes pulse gives rise to the temporal gate which markedly increases the spectral resolution compared with utilizing three unchirped femtosecond pulses. In addition, since all of the pulses originate from the same laser, this obviates the need for synchronizing two separate laser systems.

Hellerer et al. recently pursued the use of chirped pulses in CARS spectroscopy to achieve high spectral resolution and to reduce the nonresonant background by "spectrally focusing" the pump and Stokes pulses to a single vibrational mode by chirping all pulses with the same chirp rate.[7] In this technique, all portions of the chirped pulses have the same energy difference at a given delay, thereby exciting only one vibrational mode for a given delay between the pump and Stokes pulses, trading the multiplex advantage for high spectral resolution. This technically elegant technique achieves high spectral resolution through the narrow temporal overlap of the temporally dispersed frequencies in the pump, Stokes, and probe pulses which spectrally disperses the generated CARS signal for each arbitrarily small step in the temporal overlap. However, the generated CARS signal is broad due to the large energy distribution in the probe pulse, regardless of its chirp rate. Therefore, a high spectral resolution spectrum cannot be obtained by dispersing the generated signal onto a CCD, but only by stepping the relative delay between the pump and Stokes pulses (e.g., for a positive delay the "bluer" frequencies of the Stokes pulse overlap the "redder" frequencies of the pump pulse, decreasing the energy difference between the pulses). This inefficiently uses the spectral intensities of the incident pulses to generate the CARS spectrum, since large delays are required for small Raman shifts, reducing the tunability of the technique. In contrast, our technique obtains a multiplex CARS spectrum with high spectral resolution over the entire bandwidth of the femtosecond Stokes pulse in each shot, without the use of a delay, and can use the highest spectral intensity of the pump laser to generate the CARS signal, an important factor since the CARS signal intensity scales as the square of the pump power. Whereas each technique has its respective advantages, the approach to chirped CARS spectroscopy presented here is arguably the simplest and most versatile.

In this paper, we extend applications of this technique from liquid hydrocarbons to the solid state, obtaining high spectral resolution c-CARS spectra of polystyrene beads, a model system for determining the sensitivity of this technique and its applicability for CARS imaging. Next, we simulate the chirped CARS spectra of liquid hydrocarbons under different experimental conditions to show that the combination of chirped and unchirped pulses, wherein one pulse is temporally much shorter than the other pulses, generates the high spectral resolution c-CARS spectra by constituting a temporal gate. Furthermore, we explore different chirping schemes to show that the probe pulse must be of narrow spectral bandwidth to achieve high spectral resolution c-CARS spectra. Finally, the role of the chirped pulses in generating high spectral resolution spectra via a temporal gate is explored by analyzing the real and imaginary

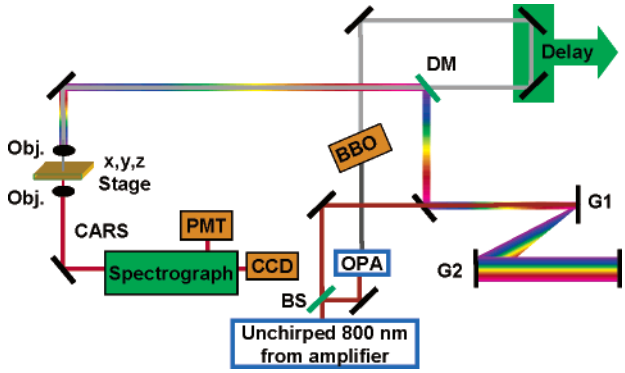


**Figure 2.** Experimental design for chirped-CARS. An unchirped 800 nm "pump/probe" pulse from the amplifier passes four times between a pair of matched gratings (G1 and G2) which generate a negative chirp in the pulse. A portion of the amplifier pulse is picked off by a beam splitter (BS) and sent to an OPA. The idler pulse from the OPA is doubled with a BBO crystal, directed through a delay stage, and overlapped spatially and temporally with the pump/probe pulse on a dichroic mirror (DM) that transmits the "Stokes" pulse and reflects the pump/probe pulse. Both beams are focused by an objective onto the sample, which is scanned through the focus by an *x*,*y*,*z* piezoelectric stage. The scattered CARS photons are collected by a matched objective and dispersed in a spectrograph onto either a CCD or PMT detector, for collecting spectra or images, respectively.

components of modeled CARS spectra employing an unchirped, broad femtosecond Stokes pulse and either chirped or unchirped degenerate pump/probe pulses to quantify the spectral resolution and to further understand the mechanism of generating high spectral resolution multiplex CARS spectra. While one advantage of the c-CARS technique is that the spectral resolution can very easily be adjusted via the grating separation to match the intrinsic line widths of the sample transitions, thereby optimizing the chemical contrast via the ratio of resonant to nonresonant CARS signal, the role of the chirp rate of the probe pulse in conjunction with the dephasing time of the vibrational state on the ultimate achievable spectral resolution will be discussed.

## Experimental Section

**Optical Setup (Figure 2).** Femtosecond pulses for the pump/probe and Stokes beams are generated by a home-built Ti:Sapphire oscillator and are amplified by a regenerative amplifier (90 fs, 1 kHz, Spectra Physics, Spitfire) before entering an optical parametric amplifier (OPA) (Light Conversion, TOPAS) that generates the near-infrared idler pulse for the Stokes beam ($\omega_s$). The degenerate pump/probe beam ($\omega_p/\omega_{p'}$) is generated by using a small amount (5%) of the s-polarized 800 nm beam from the amplifier, which is picked off by a beam-splitter before entering the OPA. This pulse makes four passes between two gratings (800 nm blaze, 830 grooves/mm, Edmund Industrial Optics), stretching the pulse in time due to the induced linear negative temporal chirp, and resulting in the blue frequencies of the pulse leading the red frequencies in time. The near-infrared (2100 nm) s-polarized idler beam from the OPA is frequency-doubled by a BBO crystal to a p-polarized 1050 nm Stokes beam, and temporally overlapped with the pump/probe beam by using a delay stage. The average powers of the pump/probe and Stokes beams can be varied from 0.02 to 10 mW and 0.02 to 2 mW, respectively. The Stokes beam is tunable from 800 to 1175 nm, corresponding to Raman shifts from 0 to 4000 $cm^{-1}$, when employing the appropriate optics for spatially overlapping the pump/probe and Stokes pulses.

To generate the CARS signal, degenerate chirped pump/probe pulses at 800 nm and the tunable unchirped near-infrared Stokes pulse at 1050 nm are spatially overlapped with a dichroic mirror (CVI) and temporally overlapped via a delay stage. The maximum overall CARS signal is defined as $t = 0$. The pulses are focused by an objective (0.9 NA or 1.2 NA, Olympus) to ca. 1 $\mu$m spot size onto the sample, placed in either a 1 mm thick cuvette or dispersed onto a No. 1 thickness (0.13 to 0.17 mm) coverslip. A matched numerical aperture (NA) objective is used to collect the scattered CARS signal centered at $2\omega_p - \omega_s \cong 650$ nm, which is then dispersed by a spectrometer and imaged on a CCD camera, collecting roughly 300 $cm^{-1}$ of the CARS vibrational spectrum in each laser shot. For imaging experiments, the sample can be scanned through the focus by an *x*,*y*,*z* translation stage (Lumina, Veeco). For collecting the CARS signal from selected vibrations, the signal dispersed in the spectrometer can be directed through a slit and onto a PMT, allowing the acquisition of chemically specific images from the sample.

**Results.** Initial proof-of-principle c-CARS spectroscopy experiments on liquid hydrocarbons were recently published.[6] The resonance enhancement achieved with high spectral resolution chirped CARS was shown to dominate the CARS spectrum of liquid methanol, with only minimal spectral distortion resulting from interference with the nonresonant electronic CARS background, a problematic artifact of nonlinear optical experiments. The observed peaks followed the expected shifts when varying the Stokes frequency, confirming resonance enhancement of the CARS signal. In addition, when the delay between the chirped $\omega_p$ pulse and the $\omega_S$ pulses was varied, the temporal gate caused the overall CARS spectrum to shift in direct proportion to the relative delay change. Since the temporal gate selects a different $\omega_p$ frequency, the center CARS wavelength shifts because it is determined by the sum of the vibrational frequencies and the probe frequency. Through these experiments, it was shown that our simple chirped pulse approach could be used to obtain high spectral resolution multiplex CARS spectra.

Previously we reported that the narrowest observed spectral resolution was achieved for liquid isooctane, wherein two transitions related to the $CH_3$ symmetric stretch appeared as two clearly resolved and reproducible peaks, with a splitting of 5 $cm^{-1}$.[6] However, when directly measuring the isooctane spectrum with a high spectral resolution spontaneous Raman spectrometer, rather than attempting to discern the possibility of a peak splitting from Raman library isooctane spectra,[24] we could not reproduce the appearance of a splitting of the 2906 $cm^{-1}$ C−H stretch.[25] Thus the apparent splitting in the c-CARS spectrum was likely an artifact caused by the CARS signal being slightly misaligned and/or out of focus upon entering the spectrograph. Therefore, liquid isooctane is not a good candidate to determine the absolute spectral resolution of the c-CARS technique.

A reliable determination of the spectral resolution of this technique is shown below for cyclohexane (Figure 3). The C−H stretches at 2942 and 2923 $cm^{-1}$ which are separated by 19 $cm^{-1}$ are clearly resolved. The full width half maximum (FWHM) line widths of these transitions are 16 and 10 $cm^{-1}$, respectively. These values compare well to their measured spontaneous Raman values of 12 and 13 $cm^{-1}$ fwhm, respectively. The narrow C−H stretch at 2853 $cm^{-1}$ appears broader than the measured spontaneous Raman value of 9 $cm^{-1}$ fwhm, but is still a relatively narrow 14 $cm^{-1}$ fwhm. In addition, a second "ringing" peak on the shoulder of the 2853 $cm^{-1}$ peak appears, which is not in the spontaneous Raman spectrum. Note how the broadening is greater and the ringing more pronounced

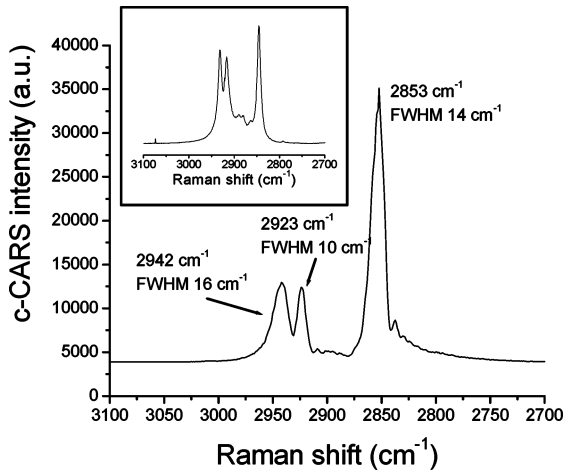


**Figure 3.** c-CARS spectrum of liquid cyclohexane. Note the two clearly resolved C−H stretches at wavenumbers of 2942 and 2923 $cm^{-1}$ with line widths of 16 and 10 $cm^{-1}$, respectively. The narrow C−H stretch at 2853 $cm^{-1}$ appears broader than the spontaneous Raman spectrum, but is still a relatively narrow 14 $cm^{-1}$ fwhm. Therefore, the spectral resolution of the c-CARS technique for a chirp rate of ca. 5 $cm^{-1}$/ps is better than 10 $cm^{-1}$. Inset: Spontaneous Raman spectrum of liquid cyclohexane.

for the intrinsically narrower transition at 2853 $cm^{-1}$. The broadening of the line width as well as the ringing peak are due to interactions of the chirped probe pulse with the dephasing of the vibrational coherence, an effect observed for narrow line width transitions and for fast chirp rates, which will be discussed below. However, it can be stated unambiguously that the spectral resolution of the c-CARS technique for a chirp rate of ca. 5 $cm^{-1}$/ps has been shown to be better than 10 $cm^{-1}$. This is a factor of 16 times better than the transform limit of the 90 fs unchirped laser pulses (163 $cm^{-1}$ fwhm bandwidth).

This technique was then extended to solid-state samples, collecting c-CARS spectra of 6 $\mu$m polystyrene beads with signal-to-noise ratios of greater than 800:1, in 4 s (Figure 4a). Within the spectral bandwidth of the experiment, the strong aromatic C−H stretch at 3054 $cm^{-1}$ and aliphatic $CH_2$ symmetric stretches at 2901 and 2851 $cm^{-1}$ can be observed in roughly the ratios expected, given the molecular structure of polystyrene (5:3). Also observed are two weak aliphatic $CH_2$ antisymmetric stretches at 2994 and 2968 $cm^{-1}$, in good agreement with their literature values.[26] Some nonresonant CARS signal is present around 3000 $cm^{-1}$; however, the resonant peaks dominate the broad nonresonant contribution. A representative c-CARS spectrum of the minimal contribution to the nonresonant background by the substrate when the focus is moved off of a bead is presented in Figure 4b.

Originally we believed the peak at 3020 $cm^{-1}$ was an aromatic C−H vibration, as previously assigned by Jasse et al. in their analysis of pulled atactic polystyrene (APS) films.[26] However, this pulled APS spectrum is different from other published Raman spectra of polystyrene in the literature. Upon careful analysis of our data, it was determined that this c-CARS peak was actually due to a ringing caused by the interactions of several frequencies in the chirped pulse generating CARS signals which interfere constructively and destructively with the dephasing coherent state of the molecule to generate a ringing to the red of the fundamental CARS peak. After probing the excited state, the red frequencies of the chirped pulse continue to probe the coherent state generated by the first two pulses, for which the dephasing time is inversely proportional to the intrinsic line

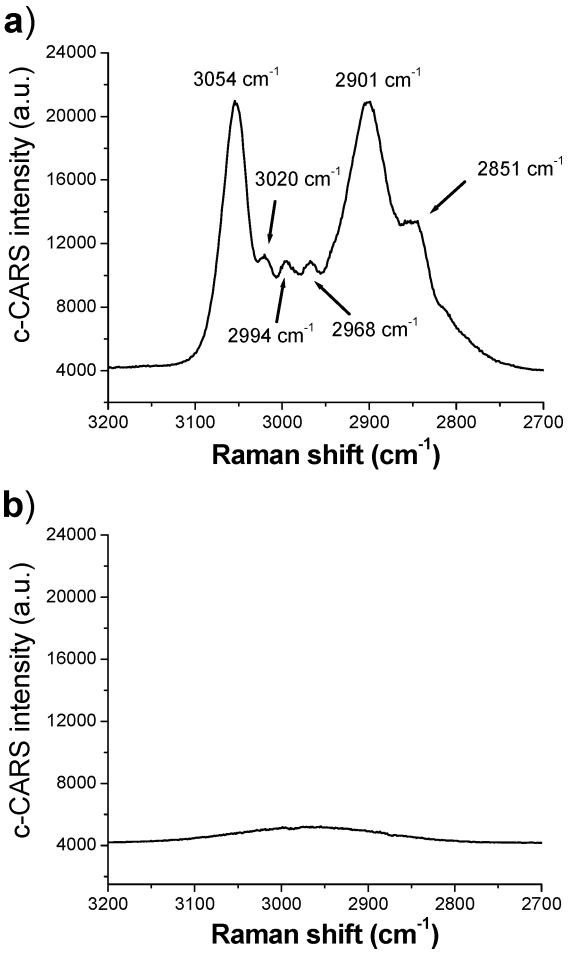


**Figure 4.** (a) c-CARS spectrum of a 6 $\mu$m polystyrene bead, $\omega_p$ = 800 nm, $\omega_S$ = 1037.5 nm, total integration time = 4 s (4000 shots), S/N >800:1. Note the aromatic C−H stretch at 3054 $cm^{-1}$, the two strong aliphatic $CH_2$ symmetric stretches at 2901 and 2851 $cm^{-1}$, and the weaker $CH_2$ antisymmetric aliphatic stretches at 2994 and 2968 $cm^{-1}$. The artifact peak at 3020 $cm^{-1}$ appears due the interference of out-of-phase CARS signals generated by the chirped probe pulse interacting with the dephasing vibrational coherence. (b) Nonresonant c-CARS spectrum taken off the bead. No interference was present since there was no dephasing of the vibrational coherence interacting with the chirped probe pulse.

width of the sample,[27]

$$\Delta\omega(\text{fwhm})\ (\text{cm}^{-1}) = \frac{1}{c\pi T_2} \qquad (2)$$

If the dephasing time is short (on the order of the pulse width of the Stokes pulse, i.e., the temporal gate), then the red frequencies of the chirped probe pulse have no effect on the observed c-CARS signals. However, if the dephasing time is on the order of the temporal length of the probe pulse after time zero (e.g., 9.4 ps/2 = 4.7 ps), then the red frequencies generate new CARS signals from the dephasing molecule. This distorts the red side of the c-CARS spectrum, showing a pronounced exponential decay shape that is distinct from the typical distortion observed in CARS spectroscopy when the nonresonant CARS signals interfere with the resonant CARS signal. In addition, due to the interfering contributions of multiple electric fields with different phases at different times, a ringing pattern in the c-CARS spectrum is observed to be convoluted with the exponential decay envelope of the dephasing transition.

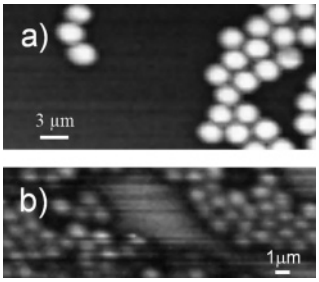


**Figure 5.** Chirped CARS microscopy images of polystyrene beads dispersed on a glass coverslip. The pump/probe pulse, centered at 800 nm, was chirped to 9.4 ps from an original pulse width of 90 fs, yielding a chirp rate of roughly 21 $cm^{-1}$/ps and effecting a spectral resolution of ca. 3 $cm^{-1}$. The Stokes pulse centered at 1050 nm was an unchirped 90 fs pulse of roughly 250 $cm^{-1}$ bandwidth. The pump/probe power was 30 $\mu$W, although only roughly 1% was actually used to generate resonant CARS signal via the temporal gate. The Stokes power was 20 $\mu$W. Both pulses occurred at a 1 kHz rep rate. Pixel dwell time was 50 ms/pixel. Contrast arises from the resonant aromatic C−H stretches in the bead. (a) c-CARS image of 3 $\mu$m polystyrene beads acquired in ca. 8 min. (b) c-CARS image of 1 $\mu$m polystyrene beads. The spatial resolution in this image is approaching the limit of the spatial resolution achievable by the 1.2 NA objectives used to focus and collect the c-CARS signal (ca. 1 $\mu$m).

This effect is more pronounced for narrow-band transitions such as the 2945 $cm^{-1}$ peak of acetonitrile probed with a fast chirp rate (ca. 21 $cm^{-1}$/ps; results not shown), for which the line width was measured to be 7 $cm^{-1}$ fwhm by spontaneous Raman and broadened to 16 $cm^{-1}$ in the c-CARS experiment, accompanied by at least seven resolvable ringing peaks. The dephasing time, $T_2$, for this transition is 5.4 ps,[27] comparable to the 4.7 ps present in the chirped probe pulse after $t = 0$. Also, when the red side of the peak is isolated from other transitions such as the 2853 $cm^{-1}$ peak of cyclohexane in Figure 3, the ringing is more readily observed. However, the measured c-CARS line width more closely matched the spontaneous Raman line width and there was little ringing present when the transition was probed with a slow enough chirp rate (ca. 5 $cm^{-1}$/ps).

A similar effect was observed in time-domain calculations of chirped four-wave mixing experiments by Duppen et al.[20] They noticed that an interference pattern appears for increasing chirp rates, especially for materials with narrow line width resonances. This pattern can be used to describe the phase of the chirped pulse. While this might be an advantageous diagnostic when employing chirped pulses to measure the dynamics of a system with a single pulse dispersed onto a CCD rather than delaying a probe pulse relative to a pump pulse, this ringing presents a challenge when quantifying c-CARS vibrational spectra. In addition, it reduces the advantage of matching the spectral resolution of the technique to the intrinsic line width of the sample in order to increase the relative resonant-to-nonresonant background, as there are more frequencies present to interfere and enhance the ringing peaks.

Initial demonstrations have been made of c-CARS imaging. A representative chemically selective image of several 3 $\mu$m diameter polystyrene beads dispersed on a glass coverslip is shown in Figure 5. Contrast in the image arises from the C−H vibrational stretches in the sample. The high ratio of resonant signal on the bead to the nonresonant signal from the coverslip (~20:1) generates the strong chemical contrast in the image. After collecting an image, the stage can be moved to a specific location in the sample to collect a CARS spectrum, as described above. For example, when the focus is positioned on a 6 $\mu$m polystyrene bead, a high signal-to-noise (800:1) resonant CARS spectrum is observed (Figure 4a). Moving the focus off of a bead yields a minimal nonresonant CARS signal from the substrate (Figure 4b). Note that there is no interference in the nonresonant CARS signal, as expected since there is no vibrational coherence associated with this signal and therefore no dephasing to interact with the chirped probe pulse. Therefore, we are able to demonstrate one of the most important proof-of-principle measurements: the ability to obtain chemically selective c-CARS images with good contrast and high spatial resolution (ca. 1 $\mu$m) and to collect point spectra at any location within the sample.

Since the c-CARS signal is routed through a spectrometer before detection for either imaging (PMT) or obtaining spectra (CCD), it is also possible to obtain images via individual vibrational stretches within the sample by closing a slit before the PMT, reducing the collected CARS signal bandwidth to a specific region. This permits spatial mapping of the CARS signal based on the aliphatic or aromatic C−H contributions, and was employed in the above image to collect signal from only the aromatic contribution of the CARS signal, which also helped improve the contrast of resonant-to-nonresonant background signals. Now that the observed CARS response has been calibrated for a known system such as polystyrene beads, the chirped CARS technique shows promise to be applied to more complex and unknown materials and biological systems for quantification of their chemical composition, such as their hydrocarbon content.

## c-CARS: Theory and Simulations

**Theoretical Background and Calculation Methods.** To model our c-CARS spectra and to better understand how chirped pulses effect high spectral resolution multiplex spectra, calculated chirped CARS spectra were generated by numerically integrating the nonlinear optical equations governing the CARS signal. The basis for calculating frequency-space chirped and unchirped CARS spectra has been previously described by Cheng et al., which was followed closely here.[16] In general, the induced polarization in the sample can be expanded as a power series in terms of the electric field with the appropriate susceptibilities[28]

$$P \propto \chi^{(1)}E + \chi^{(2)}E^2 + \chi^{(3)}E^3 + ... \quad (3)$$

where $\chi^{(n)}$ is the susceptibility tensor of rank $n + 1$. CARS is a third-order process, therefore the third term governs the CARS signal. Writing it in the frequency domain offers a convenient description for taking into account the material susceptibilities.[29] In this case, the third-order induced polarization is written as

$$P^{(3)}(\omega_{as}) = \int_{-\infty}^{+\infty}d\omega_p\int_{-\infty}^{+\infty}d\omega_s\int_{-\infty}^{+\infty}d\omega_{p'}\chi^{(3)}_{1111}(-\omega_{as};\omega_p,-\omega_s,\omega_{p'}) \times E_p(\omega_p)E_s(\omega_s)E_{p'}(\omega_{p'})\delta(\omega_p - \omega_s + \omega_{p'} - \omega_{as}) \quad (4)$$

where $\chi^{(3)}_{1111}$ is the parallel pump/probe component of the susceptibility; $E_p(\omega_p)$, $E_s(\omega_s)$, and $E_{p'}(\omega_{p'})$ are the electric fields for the pump, Stokes, and probe pulses, respectively; and $\delta(\omega_p - \omega_S + \omega_{p'} - \omega_{as})$ ensures energy conservation. Integration of the delta function defines the relationship between the pump, probe, and Stokes frequencies ($\omega_{as} = \omega_p - \omega_s + \omega_{p'}$). Now, each variable ($\omega_p$, $\omega_s$, $\omega_{p'}$, $\omega_{as}$) can be written in terms of the other variables, specifically $\omega_s$ in terms of $\omega_p$, $\omega_{p'}$, and $\omega_{as}$, and therefore eq 4 becomes

$$P^{(3)}(\omega_{as}) = \int_{-\infty}^{+\infty} d\omega_p \int_{-\infty}^{+\infty} d\omega_{p'} \chi^{(3)}_{1111}(-\omega_{as};\omega_p,-\omega_s,\omega_{p'}) \times E_p(\omega_p)E_s(\omega_s)E_p(\omega_{p'}) \quad (5)$$

In the calculations, the electric fields are assumed to have a Gaussian spectral intensity envelope and can be either chirped or unchirped (i.e., transform-limited). For our experimental setup, the pump and probe fields are degenerate and are linearly chirped, described by the equation[30]

$$E_p(\omega_p) = E_p \exp\left[-\frac{1}{4}\left(\frac{a}{a^2+b^2}\right)(\omega_p - \omega_{po})^2 - \frac{i}{4}\left(\frac{a}{a^2+b^2}\right)(\omega_p - \omega_{po})^2\right] \quad (6)$$

where $E_p$ is the peak amplitude of the field, $\omega_{po}$ is the central frequency of the pump/probe field, and $a$ and $b$ are parameters that describe the envelope of the electric field and the measure of the chirp, respectively. The effect of these parameters on the electric field is more readily apparent in the time domain

$$E(t) = \exp(-at^2) \exp[i(\omega_0 t + bt^2)] \quad (7)$$

where $a$ describes the envelope function of the electric field and therefore the temporal fwhm pulse width ($\tau$) as given by $a = 2\ln 2/\tau^2$, and $b$ describes the relative phase shift between the frequencies in the pulse. The parameters $a$ and $b$ are related by the expression $b = a(R^2 - 1)^{1/2}$, where $R$ is the ratio of the chirped to transform-limited temporal fwhm pulse widths, as defined by Cheng et al.[16] For a transform-limited (unchirped) pump/probe pulse, $R$ equals 1.0 and

$$\tau = \left(\frac{2\ln 2}{\pi}\right)\left(\frac{2\pi}{\Delta\omega_p}\right) = \left(\frac{4\ln 2}{\Delta\omega_p}\right) \quad (8)$$

where $\Delta\omega_p$ is the fwhm spectral bandwidth (in radians/second) of the pulse. In this case, eq 6 simplifies to

$$E_s(\omega_s) = E_s \exp\left[-2\ln 2\left(\frac{\omega_s - \omega_{so}}{\Delta\omega_s}\right)^2\right] \quad (9)$$

which describes the unchirped, transform-limited Gaussian Stokes pulse. The spectral bandwidth $\Delta\omega_s$ determines the multiplex spectral bandwidth for the experimental setup described above.

The susceptibility term, $\chi^{(3)}_{1111}$, includes nonresonant and resonant terms[31]

$$\chi^{(3)}_{1111} = \chi^{nr}_{1111} + \sum_j \chi^{r}_{1111} \quad (10)$$

where $\chi^{nr}_{1111}$ is the nonresonant electronic background susceptibility, a constant far from electronic resonances, and the resonant contribution, $\chi^{r}_{1111}$, summed over all the Raman-active modes

$$\chi^{r}_{1111}(\omega_p - \omega_s) = \sum_j \frac{A_j}{\Omega_j - (\omega_p - \omega_s) - i\Gamma_j} \quad (11)$$

where $A_j$ is related to the spontaneous Raman cross-section, $\Omega_j$ is the Raman vibrational frequency, $(\omega_p - \omega_s)$ is the energy difference between the pump and Stokes pulses, which determines the resonance enhancement, and $\Gamma_j$ is the half-line width of the Raman transition. For isotropic media, all the different polarization orientations for the molecular susceptibility can be written in terms of the all-parallel case, and since the polarization of the incident pulses does not affect the spectral resolution arising from chirped pulses, the calculations written in terms of the all parallel case faithfully reproduce the experiments.

The simulated CARS spectra were based on the parameters defined by the physical constraints of the experimental design and the sample, and the theoretical equations described above. These include specification of which pulses were chirped and their chirp rate, the observed line widths and vibrational frequencies of the measured Raman transitions, and the observed relative ratio of resonant to nonresonant background. The overall CARS spectrum was generated by taking the squared modulus of the induced polarization described in eq 5, which contains both real and imaginary terms due to the molecular susceptibility and, if the pulses are chirped, the phase of the chirp from eq 6, as shown in eq 12,

$$I_{CARS}(\omega_{as}) = |P^{(3)}(\omega_{as})|^2 \quad (12)$$

The key for successfully utilizing nonlinear spectroscopic techniques is to increase the contribution of the resonant component relative to the nonresonant background. In the present case, careful control of the grating spacing to adjust the chirp rate can make the spectral resolution match the intrinsic line widths of the sample, thereby increasing the resonant component. However, as described in detail below, our calculations show that chirped pulses do not resolve CARS spectra as cleanly as unchirped, narrow-bandwidth pulses when the experiment is not in the intrinsic line width-limiting case. A similar situation was briefly discussed by Richter et al. for using chirped pulses to generate high spectral resolution multiplex sum frequency signals.[19] Therefore, when using chirped pulses to achieve high spectral resolution CARS, there appears to be a tradeoff between achieving undistorted spectra with high spectral resolution and increasing the resonant signal by matching the spectral resolution to the intrinsic line width of the sample. Also as mentioned above, interference between the red frequencies of the chirped probe pulse and the dephasing of the vibrational coherence can result in a line-broadened, ringing c-CARS spectrum. A time domain calculation of the chirped CARS spectrum would be necessary to fully describe this effect due to the inability of the frequency space representation to account for the dephasing times of the vibrational coherence. For the present, the frequency space calculations adequately describe the effect of the creation of a temporal gate to achieve high spectral resolution CARS spectra.

**Simulated c-CARS Spectra vs Experimental Results.** The above equations were used to calculate a chirped CARS spectrum for liquid methanol (Figure 6). The pump/probe frequency was set to 12 500 $cm^{-1}$ (800 nm), originally a transform-limited 90 fs pulse stretched to 53.1 ps by a linear negative chirp. The Stokes pulse is defined as an unchirped pulse at 9524 $cm^{-1}$ (1050 nm) with 250 $cm^{-1}$ bandwidth, comparable to the observed spectral bandwidth of the experimental Stokes pulse. The full-width half-maximum (fwhm) line widths of the asymmetric (2944 $cm^{-1}$) and symmetric (2836 $cm^{-1}$) C−H stretches were 34 and 21 $cm^{-1}$, respectively, comparable to those measured by spontaneous Raman spectroscopy in our lab (36 and 20 $cm^{-1}$ fwhm, respectively). The relative ratio of resonant to nonresonant background was 200:1. For liquid methanol, the calculated c-CARS spectrum matches the experimental result almost exactly, except for the asymmetric line shape of the 2944 $cm^{-1}$ peak, which is also present in the spontaneous Raman spectrum. Also note the lack of "ringing" in the experimental c-CARS liquid methanol spectrum, which shows that for a slow

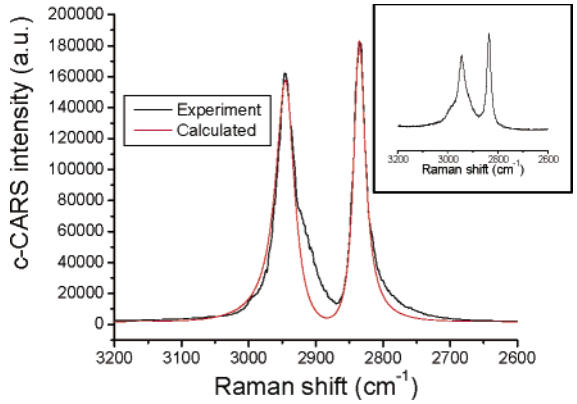


**Figure 6.** Overlaid experimental and calculated c-CARS spectra for the symmetric and asymmetric $CH_3$ stretches for liquid methanol. A degenerate pump/probe wavelength of 800 nm chirped from 90 fs to 53.1 ps (chirp rate ca. 5 cm$^{-1}$/ps) and an unchirped 90 fs Stokes wavelength of 1050 nm were used both experimentally and in the calculations. Insert: Spontaneous Raman spectrum for liquid methanol.

chirp rate and broad intrinsic line width (and subsequent short dephasing time), the ringing becomes negligible. The calculations clearly show that the chirping of the probe pulse provides an effective narrowing of the spectral bandwidth of the original 90 fs pulse (163 cm$^{-1}$ fwhm if transform limited) to less than the intrinsic line width of the liquid methanol stretches, resulting in the high spectral resolution c-CARS spectrum.

Calculations also closely matched the experimental results for decreased chirp rate of the pump/probe pulses, wherein the pulses were chirped from 90 fs to 22.4 and 53.1 ps (see Figure 7). In both cases, the intrinsic line widths of the methanol stretches are greater than the spectral resolution of the technique, calculated to be ca. 1 and 0.4 cm$^{-1}$ for chirped pulse widths of 22.4 and 53.1 ps, respectively, by eq 1. Therefore the chirp rate did not affect the observed line widths for all three chirped conditions, and the traces closely overlap since they are intrinsic line width limited. Subtle differences in the experimental results are due to generating CARS signal from slightly different Stokes center wavelengths, which changes the relative peak height of the two methanol stretches.

Additionally, for the previously reported experimental results wherein the Stokes wavelength was varied while holding the pump/probe wavelength constant, and which confirmed resonance enhancement of the chirped CARS signal for liquid methanol stretches, the c-CARS calculations faithfully reproduced those results (see Figure 8).[6] As the experimental results showed, the calculated chirped CARS wavelength is the same for each C−H resonance, even though the relative contribution from the nonresonant CARS signal increased as the difference between the pump/probe and Stokes wavelengths moved further from the resonances. Additional experimental results for adjusting the pump/probe delay relative to the Stokes pulse that were previously reported were not reproduced with our calculations since there is no provision in our current model for adjusting relative delay between the pulses in the frequency-space derivation of the generated CARS signal. Those experimental results showed that changing the relative delay caused the overall CARS spectrum to shift, and confirmed that the temporal gate was generating the high spectral resolution c-CARS spectra in the limiting case where the Stokes pulse is temporally much shorter than the chirped pump/probe pulse, the dephasing time of the coherent state is short compared to the temporal extent of the probe pulse, and the chirp rate of the probe pulse is slow. In our calculations the temporal overlap is always assumed to

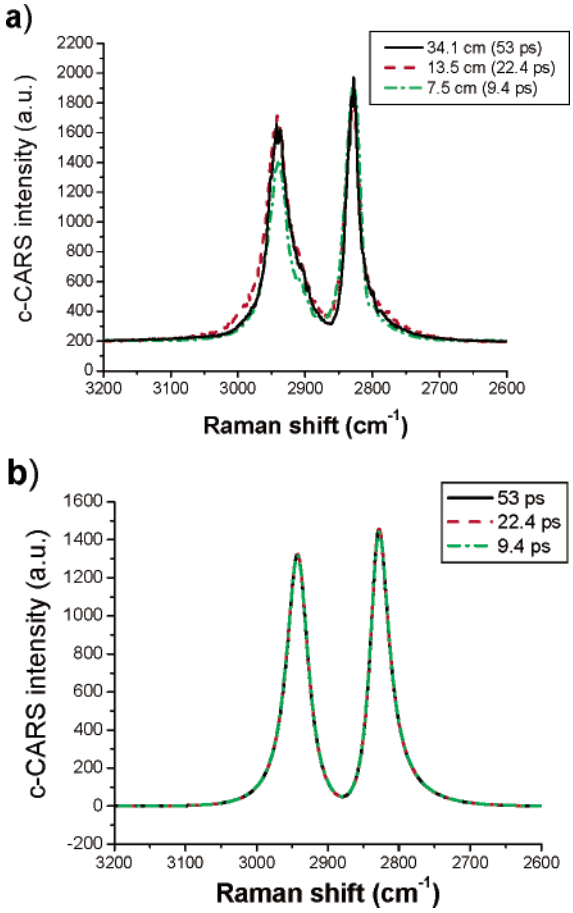


**Figure 7.** Chirped CARS spectra of liquid methanol for three different grating separations, with their corresponding measured (stretched) pulse widths. In each case the spectral resolution achieved by the chirped pulses is smaller than the intrinsic line widths of liquid methanol, therefore the chirp rate does not affect the observed line widths and thus all spectra directly overlap. (a) Degenerate pump/probe wavelength of 804.1 nm chirped from 90 fs to 53, 22.4, and 9.4 ps and unchirped 90 fs Stokes wavelength of 1050 nm. (b) Calculated liquid methanol spectra for the same experimental conditions.

occur at time zero (maximum signal) with no relative delay. Future work in time/frequency space, where the relative delay between pulses can be adjusted, will allow for further calculations of delay-based experiments, in addition to further quantifying the spectral resolution when the dephasing time of the vibrational state is long, as is the case for transitions with narrow line widths. Nevertheless, the frequency space calculations explain the effect of chirped pulses in generating high spectral resolution quite well.

**Chirping Scheme.** To illustrate the importance of using the correct chirping scheme for generating high spectral resolution c-CARS spectra (i.e., the probe pulse is spectrally narrow), experiments and calculations were performed wherein the Stokes pulse was chirped and the pump/probe pulses were unchirped. For this experiment, the "signal" pulse from the OPA was doubled from 1300 to 650 nm (15 383 cm$^{-1}$) to provide the degenerate unchirped pump and probe pulses of 90 fs duration (and thus spectrally broad). A chirped 800 nm pulse (12 500 cm$^{-1}$) was used for the Stokes pulse, stretched temporally to 15.8 ps duration from the original 90 fs fwhm pulse width. The frequency difference between the pump and Stokes pulses matched the vibrational frequencies of the C−H stretches of liquid methanol for resonant enhancement. However, in this configuration, an unresolved, broad spectrum was observed for

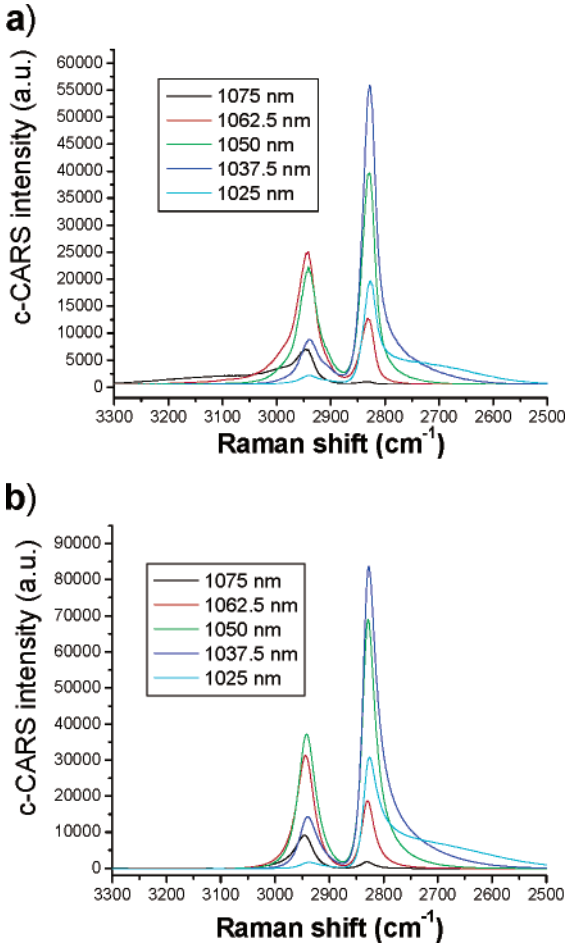


**Figure 8.** c-CARS spectra obtained for different Stokes wavelengths while holding the pump/probe wavelength constant at 801.9 nm. (a) Experimental results wherein resonance enhancement are confirmed, since the C−H stretches appear at the same CARS wavelength even as the relative nonresonant contribution increases on each side of the spectrum as the difference between the pump/probe and Stokes wavelengths shifts off resonance. (b) Similar results for the calculated c-CARS spectra.

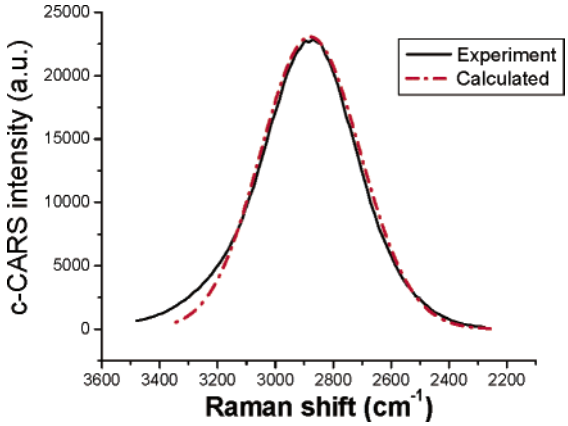


**Figure 9.** Experimental and chirped CARS spectra of liquid methanol employing unchirped 90 fs pump/probe pulses at 650 nm and a chirped Stokes pulse at 800 nm stretched from 90 fs to 15.8 ps duration. The vibrations are unresolved in both cases, showing that the probe pulse must be spectrally narrow to achieve high spectral resolution multiplex CARS spectra.

both the experimental and calculated CARS spectra (see Figure 9). Therefore, employing an unchirped femtosecond probe pulse will result in low spectral resolution, the result of an incorrect chirping scheme for generating c-CARS spectra.

This can be understood by viewing the CARS process in a stepwise fashion. The pump ($\omega_p$) pulse can be of either broad or narrow bandwidth, exciting many or few "virtual" states, as Figure 1 shows for the energy level diagram for polystyrene. The Stokes pulse can also possess either a narrow or broad bandwidth, creating a coherence of multiple vibrational states, the number of which depends on the spectral bandwidths of the pump and Stokes pulses, as well as the density of Raman active vibrational modes. If both pump and Stokes pulses are spectrally narrow, there is no multiplex advantage since only a small number (possibly one or none) of vibrational states are excited. If one of the pump or Stokes pulses are spectrally broad, then multiple states will be excited, depending on the bandwidth. If both the Stokes and pump pulses are broad, the number of excited vibrational energy states is determined by the convolution of the bandwidths of the two pulses (and the mode density).

The probe pulse resolves the coherent superposition of excited vibrational states. If the probe pulse is spectrally broad, it essentially scrambles the signal from the discreet vibrational energy levels, since multiple frequencies in the probe pulse can resolve each vibrational energy level, thereby generating an unresolved CARS spectrum. This will occur regardless of how spectrally broad or narrow the initial pump and Stokes pulses were in generating the excited vibrational energy levels. However, if the probe pulse is spectrally narrow, either because its transform-limited bandwidth is smaller than the intrinsic line width of the vibrational energy levels that it is resolving, or because the pulse is chirped to a sufficient extent that the effective spectral bandwidth is less than the intrinsic line width, then a resolved multiplex CARS spectrum will appear. In this case, the narrow probe pulse acts like a narrow spectral window that resolves a slice of each excited coherent state, either on or off a vibrational resonance, at a spectral resolution equal to the bandwidth or effective bandwidth of the pulse. This is the mechanism that generates high spectral resolution multiplex CARS spectra when employing femtosecond pulses with the correct chirping scheme.

**Modeling c-CARS Spectra.** The CARS signal contains both real and imaginary components; therefore, comparing the relative contribution from each yields additional insight into the structure of the observed CARS spectrum, such as the differences between achieving high spectral resolution CARS spectra utilizing chirped femtosecond pump/probe pulses compared to using intrinsically spectrally narrow picosecond pulses. This comparison helps to quantify the spectral resolution of the c-CARS technique. The temporal gate model predicts that the probe pulse should contribute roughly 1.6 $cm^{-1}$ to the achieved spectral resolution, as determined by eq 1 (0.09 ps/9.4 ps × 163 $cm^{-1}$ = 1.6 $cm^{-1}$). However, when comparing calculated CARS spectra employing chirped femtosecond probe pulses to unchirped picosecond probe pulses with equivalent spectral bandwidth, the unchirped CARS spectra are slightly better resolved than the c-CARS spectra (results not shown). Unchirped spectral bandwidths of ca. 3 $cm^{-1}$ more closely match the chirped probe pulse results. This can be understood by examining the real contribution of the chirped pulse electric field to the spectral bandwidth. When the values for $a$ and $b$ for a 90 fs pulse chirped to 9.4 ps are inserted into eq 6, the real part of the equation simplifies to the unchirped eq 9, with $(1/R)$ times the spectral bandwidth

$$E_s(\omega_s) = E_s \exp\left[-2\ln 2\left(\frac{\omega_s - \omega_{so}}{(1/R)\Delta\omega_s}\right)^2\right] \qquad (13)$$

Therefore, for a 90 fs pulse of 163 $cm^{-1}$ fwhm bandwidth

linearly chirped to 9.4 ps, the real component of the chirped pulse contributes 1.6 $cm^{-1}$ to the overall spectral bandwidth. This analysis does not take into account the imaginary contribution of the chirped field to the spectral resolution, which would be comparable to the real contribution, thereby increasing the spectral bandwidth contribution of a chirped pulse relative to an unchirped pulse. The temporal gate model only takes into account the real contribution, therefore it underestimates the overall contribution of the chirped pump/probe pulse electric field.

To better understand how the probe pulse determines the spectral resolution, CARS spectra of liquid methanol were modeled for increasing spectral bandwidths of unchirped pump/probe pulses (from 5 to 163 $cm^{-1}$), while holding the spectral bandwidth of the unchirped 90 fs Stokes pulse constant at 163 $cm^{-1}$ fwhm (Figure 10). For spectral bandwidths that were less than the intrinsic line widths, the two vibrational peaks were clearly resolved, as observed in the c-CARS experiments described above. The real contribution to the observed CARS spectrum appeared as two derivative-shaped peaks with inflection points centered at the resonance frequencies of the C−H stretches (2944 and 2836 $cm^{-1}$), similar to what is observed for the real portion of the refractive index near absorptions (Figure 10b). The imaginary contribution to the CARS spectrum appeared very similar to the observed CARS spectrum, with two peaks centered at the resonance frequencies (Figure 10c). When the spectral bandwidth was increased, the peaks became increasingly broader and less resolved. It is apparent from the real contribution to the spectrum that the overall spectrum should be less resolved, since the two derivative shaped peaks blended into one, which would correspond to only one absorption in the spectrum. The two peaks in the imaginary contribution became less resolved as well. For the case where the spectral bandwidth was equal to a transform-limited 90 fs pulse (ca. 163 $cm^{-1}$ fwhm), the two transitions in the CARS spectrum were completely unresolved, with the maximum in the observed CARS spectrum appearing between the two transitions. Overall, as the bandwidth of the unchirped pump/probe pulse is increased, the simulated CARS spectrum of liquid methanol employing three unchirped pulses smoothly evolves from having two clearly resolved peaks to exhibiting one broad, unresolved peak.

When performing similar calculations with chirped pump/probe pulses with increasing chirp rates (effectively increasing the spectral bandwidth) and an unchirped 90 fs (163 $cm^{-1}$ fwhm) Stokes pulse, it was evident that the chirp rate of the probe pulse defines the spectral resolution of the technique, as shown for the normalized chirped CARS spectra in Figure 11; however, there were differences in the observed structure of the overall CARS spectrum and in both the real and imaginary components that generated the observed spectrum. As previously discussed for the chirped CARS spectra experimentally measured in this work, wherein the probe pulses were chirped by factors greater than 100, with a corresponding chirp rate of ca. 17 $cm^{-1}$/ps, the calculations matched the experiments since the spectra are intrinsic line width limited. However, when the pulses are only chirped by a factor of 10, to ca. 1 ps and with a corresponding increase in the chirp rate, the effective spectral resolution was near 20 $cm^{-1}$ fwhm, comparable to the line width of the methanol stretches. In this case, the peaks became slightly less resolved, but still retained their original line shape.

For pulses chirped by a factor of 3 to 0.25 ps with a corresponding chirp rate of ca. 650 $cm^{-1}$/ps, the effective spectral resolution of 60 $cm^{-1}$ was greater than the fwhm line width of the transitions (ca. 20−40 $cm^{-1}$). The real contribution lost most of its derivative shape and was positive for most of the spectrum (Figure 11b). The origin of the "shoulder" at 3054 $cm^{-1}$ in the CARS spectrum is now apparent as a result of the distortion in the real contribution on the blue end of the spectrum. Similarly, the imaginary spectrum was distorted as well (Figure 11c), becoming more derivative shaped with the opposite sign of the real contribution, including an inflection point at 2885 $cm^{-1}$, which resulted in the prominent "center" peak in the CARS spectrum at that frequency. A negative imaginary contribution to the CARS spectrum was a counterintuitive result and a marked difference from the spectra of the imaginary components for the unchirped CARS spectra in Figure 10.

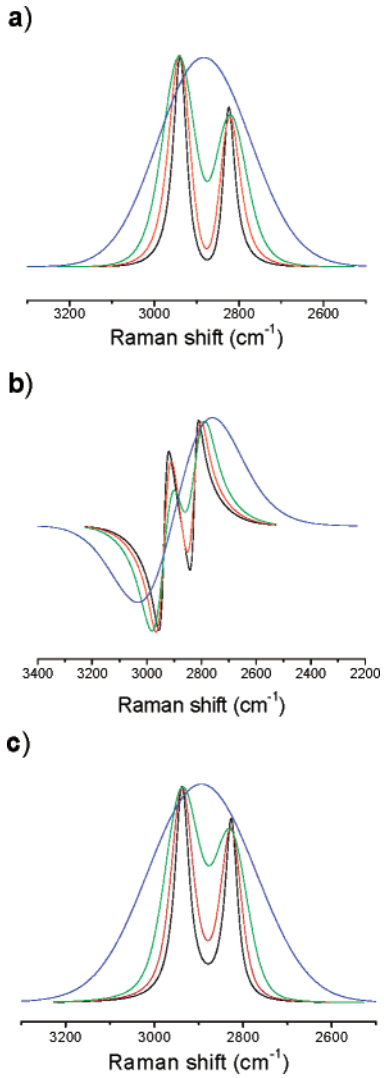


**Figure 10.** Calculated CARS spectrum of liquid methanol plus the real and imaginary components for unchirped pump/probe and 90 fs (163 $cm^{-1}$) Stokes pulses. For all three panels, the spectral bandwidth fwhm for the pump/probe pulse was the following: 5 $cm^{-1}$, black; 25 $cm^{-1}$, red; 50 $cm^{-1}$, green; and 163 $cm^{-1}$, blue. (a) CARS spectra with unchirped pulses of increasing spectral bandwidth for the pump/probe pulses. The vibrational transitions become increasingly less resolved as the spectral bandwidth increases beyond the intrinsic line width. (b) The real component of the unchirped CARS spectrum. The spectra smoothly evolve from two separate derivative shaped peaks into one for increased spectral bandwidth of the unchirped pulses, ultimately contributing to an unresolved CARS spectrum. (c) The imaginary component of the unchirped CARS spectrum. The spectra smoothly evolve from two resolved peaks to one unresolved peak for increased spectral bandwidth of the unchirped pulses.

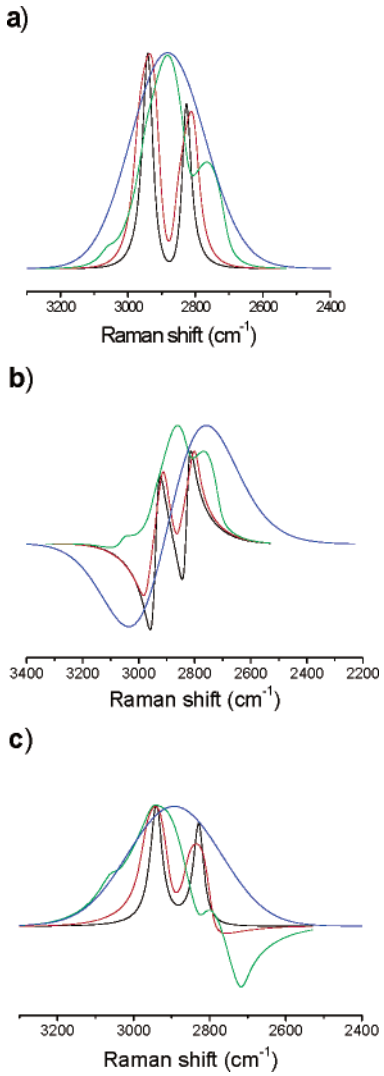


**Figure 11.** Calculated CARS spectrum plus the real and imaginary components for chirped pump/probe and unchirped 90 fs (163 $cm^{-1}$) Stokes pulses. For all three panels, the pump/probe pulse was chirped from 90 fs to 9.4 (~3 $cm^{-1}$ spectral resolution; black), 1 (~20 $cm^{-1}$; red), 0.25 (~60 $cm^{-1}$; green), and 0.09 ps (~163 $cm^{-1}$, unchirped; blue). (a) CARS spectrum for increasing chirp rate (decreasing effective spectral resolution) of the pump/probe pulse. The spectral resolution of the CARS spectrum decreases and the two transitions in liquid methanol become increasingly unresolved. (b) The real component of the chirped CARS spectrum. For increasing chirp rate, the real contribution becomes increasingly positive and distorted until the pulse is no longer chirped. (c) The imaginary component of the chirped CARS spectrum. For increasing chirp rate, the imaginary component becomes more derivative shaped and increasingly distorted, until the pulse is no longer chirped.

In the limiting case of an unchirped probe pulse, both the real and imaginary contributions were smoothly varying, and a completely unresolved CARS spectrum appears. Therefore, when employing chirped pump/probe pulses to achieve high spectral resolution CARS spectra, the effective spectral resolution needs to be less than the intrinsic line widths of the transitions, otherwise a distorted CARS spectrum will appear. These modeled spectra show that chirped pulses do not resolve CARS spectra as cleanly as unchirped, narrow-bandwidth pulses when the experiment is not in the intrinsic line width-limiting case.

This difference in these two approaches to achieving high spectral resolution is explained by the fact that for unchirped multiplex CARS, a narrow spectral bandwidth pulse is required to achieve high spectral resolution, using only a few frequencies to map out the transition. However, in chirped multiplex CARS, having a slow chirp rate (5 $cm^{-1}$/ps) over the transition is effectively the same as using fewer frequencies in the pulse. More explicitly, the chirp rate of the probe pulse times the temporal pulse width of the Stokes pulse defines the spectral resolution, since that determines the number of frequencies present to resolve the vibrational coherence. In general, this holds true when the dephasing of the vibrational dephasing is taken into account. If the dephasing time is 1 ps, only ca. 5 $cm^{-1}$ of the probe pulse contributes to the signal. In the case of a long dephasing time of the vibrational coherence (e.g., 5−10 ps), this decay contributes significantly to the temporal gate and the spectral resolution is now a convolution of the Stokes pulse width and the dephasing time. When that spectral bandwidth is sufficiently less than the intrinsic line width of the transition in the sample, the observed c-CARS spectrum is intrinsic line width limited. However, pulses with a fast chirp rate will have many rapidly varying frequencies over the spectral bandwidth used to project the vibrational coherence, causing distortion of the c-CARS peak and low spectral resolution. Therefore, to achieve high spectral resolution and cleanly resolved c-CARS spectra, the chirp rate of the probe pulse times the Stokes pulse width needs to be less than the intrinsic line width of the transition.

## Conclusions

We have shown that the two-pulse chirped-CARS technique allows for very simple control of experimental spectral resolution and chemical selectivity. The novelty of the technique is that it renders explicit bandwidth reduction unnecessary, instead exploiting only the chirp of the probe pulse to achieve high spectral resolution. As with other multiplex CARS techniques, by dispersing the CARS signal onto a CCD, we can observe the entire (ca. 300 $cm^{-1}$) CARS spectrum in a single laser shot without the need for adjusting the delay of the pulses, thereby allowing for reliable direct comparisons between peak intensities within the broadband region of interest. Through the use of diffraction gratings to induce the linear chirp, we can readily adjust the experimental spectral resolution to match the sample line widths, thus optimizing the ratio of resonant-to-nonresonant CARS signals through more efficient use of the laser power. However, as described above, distortions to the spectra can occur if the pulses have too fast of a chirp rate in relation to the dephasing time of the molecule, which can then result in an interference pattern with an exponential decay envelope function appearing on the red side of the CARS signal. Calculated chirped CARS spectra match the experimental results quite closely and yield insight into how the chirped pulses achieve high spectral resolution through mapping out the real and imaginary contributions to the total CARS signal. The simplicity of this experimental design enables high spectral resolution CARS spectra to be easily obtained with femtosecond laser systems; c-CARS should prove useful for high spatial resolution imaging with chemically selective contrast.

**Acknowledgment.** The authors thank Justin Johnson, Jared Smith, Poul Petersen, and Abigail Miller for helpful discussions and experimental developments. This work was supported in part by the Experimental Physical Chemistry Program of the National Science Foundation. This work was performed in part under the auspices of the U.S. Department of Energy by University of California Lawrence Livermore National Laboratory under contract No. W-7405-Eng-48.

## References and Notes

(1) Duncan, M. D.; Reintjes, J.; Manuccia, T. J. *Opt. Lett.* **1982**, *7*, 350.
(2) Zumbusch, A.; Holtom, G. R.; Xie, X. S. *Phys. Rev. Lett.* **1999**, *82*, 4142.
(3) Müller, M.; Schins, J. M. *J. Phys. Chem. B* **2002**, *106*, 3715.
(4) Cheng, J.-X.; Xie, X. S. *J. Phys. Chem. B* **2004**, *108*, 827.
(5) Volkmer, A. *J. Phys. D*: *Appl. Phys.* **2005**, *38*, R59.
(6) Knutsen, K. P.; Johnson, J. C.; Miller, A. E.; Petersen, P. B.; Saykally, R. J. *Chem. Phys. Lett.* **2004**, *387*, 436.
(7) Hellerer, T.; Enejder, A. M. K.; Zumbusch, A. *Appl. Phys. Lett.* **2004**, *85*, 25.
(8) Dudovich, N.; Oron, D.; Silberberg, Y. *Nature* **2002**, *418*, 512.
(9) Marks, D. L.; Vinegoni, C.; Bredfeldt, J. S.; Boppart, S. A. *Appl. Phys. Lett.* **2004**, *85*, 5787.
(10) Porter, R.; Shan, F.; Guo, T. *Rev. Sci. Instrum.* **2005**, *76*, 043108.
(11) Volkmer, A.; Cheng, J.-X.; Xie, X. S. *Phys. Rev. Lett.* **2001**, *87*, 023901.
(12) Song, J. J.; Eesley, G. L.; Levenson, M. D. *Appl. Phys. Lett.* **1976**, *29*, 567.
(13) Cheng, J.-X.; Book, L. D.; Xie, X. S. *Opt. Lett.* **2001**, *26*, 1341.
(14) Potma, E. O.; Xie, X. S. *J. Raman Spectrosc.* **2003**, *34*, 642.
(15) Evans, C. L.; Potma, E. O.; Xie, X. S. N. *Opt. Lett.* **2004**, *29*, 2923.
(16) Cheng, J.-X.; Volkmer, A.; Book, L. D.; Xie, X. S. *J. Phys. Chem. B* **2002**, *106*, 8493.
(17) Holtom, G. R.; Thrall, B. D.; Chin, B. Y.; Wiley: H. S.; Colson, S. D. *Traffic* **2001**, *2*, 781.
(18) Kee, T. W.; Cicerone, M. T. *Opt. Lett.* **2004**, *29*, 2701.
(19) Richter, L. T.; Petralli-Mallow, T. P.; Stephenson, J. C. *Opt. Lett.* **1998**, *23*, 1594.
(20) Duppen, B.; de Hann, F.; Nibbering, E. T. J.; Wiersma, D. A. *Phys. Rev. A* **1993**, *47*, 5120.
(21) Lozovoy, V. V.; Grimberg, B. I.; Brown, E. J.; Pastirk, I.; Dantus, M. *J. Raman Spectrosc.* **2000**, *31*, 41.
(22) Bartels, R. A.; Weinacht, T. C.; Leone, S. R.; Kapteyn, H. C.; Murnane, M. M. *Phys. Rev. Lett.* **2002**, *88*, 033001.
(23) Lang, T.; Motzkus, M. *J. Opt. Soc. Am. B* **2002**, *19*, 340.
(24) SDBSWeb: http://www.aist.go.jp/RIODB/SDBS/(National Institute of Advanced Industrial Science and Technology, 7/12/05).
(25) The spontaneous Raman spectrum was obtained by exciting liquid methanol contained in a 20 mm path length cuvette with the 514.532 nm laser line of an Ar+ ion laser. The Raman scattered light was collected orthogonally to the excitation angle and the Raleigh scattered light was filtered by a notch filter. The light was dispersed by a 1200 grooves/mm grating in a 0.5 m spectrograph and detected on a liquid nitrogen cooled CCD array. The spectrometer was calibrated prior to collecting the Raman spectra with a Ne lamp.
(26) Jasse, B.; Chao, R. S.; Koenig, J. L. *J. Polym. Sci., Polym. Phys. Ed.* **1978**, *16*, 2157.
(27) George, S. M.; Auweter, H.; Harris, C. B. *J. Chem. Phys.* **1980**, *73*, 5573.
(28) Nibler, J. W.; Pubanz, G. A. Coherent Raman spectroscopy of gases. In *Advances in Nonlinear Spectroscopy*; Clark, R. J. H., Hester, R. E., Eds.; John Wiley & Sons Ltd.: New York, 1988; Vol. 15, p 1.
(29) Gomez, J. S. Coherent Raman Spectroscopy. In *Modern Techniques in Raman Spectroscopy*; Laserna, J. J., Ed.; John Wiley & Sons Ltd.: New York, 1996; p 305.
(30) Siegman, A. E. *Lasers*; University Science Books: Sausalito, CA, 1986.
(31) Brakel, R.; Schneider, F. W. Polarization CARS spectroscopy. In *Advances in Nonlinear Spectroscopy*; Clark, R. J. H., Hester, R. E., Eds.; John Wiley & Sons Ltd.: New York, 1988; Vol. 15, p 149.